



**HAL**  
open science

## Vibration energy harvesting on a drone quadcopter based on piezoelectric structures

Matthias Perez, Kevin Billon, Tony Gerges, J.-F. Capsal, Michel Cabrera,  
Simon Chesné, Claire Jean-Mistral

► **To cite this version:**

Matthias Perez, Kevin Billon, Tony Gerges, J.-F. Capsal, Michel Cabrera, et al.. Vibration energy harvesting on a drone quadcopter based on piezoelectric structures. *Mechanics & Industry*, 2022, 23, pp.20. 10.1051/meca/2022021 . hal-03755140

**HAL Id: hal-03755140**



**<https://hal.science/hal-03755140v1>**

Submitted on 21 Aug 2022

**HAL** is a multi-disciplinary open access archive for the deposit and dissemination of scientific research documents, whether they are published or not. The documents may come from teaching and research institutions in France or abroad, or from public or private research centers.

L'archive ouverte pluridisciplinaire **HAL**, est destinée au dépôt et à la diffusion de documents scientifiques de niveau recherche, publiés ou non, émanant des établissements d'enseignement et de recherche français ou étrangers, des laboratoires publics ou privés.

# Vibration energy harvesting on a drone quadcopter based on piezoelectric structures

Matthias Perez<sup>1</sup>, Kevin Billon<sup>1</sup>, Tony Geroges<sup>2</sup> , Jean-Fabien Capsal<sup>3</sup>, Michel Cabrera<sup>2</sup>, Simon Chesné<sup>1,\*</sup> , and Claire Jean-Mistral<sup>1</sup>

<sup>1</sup> Univ Lyon, INSA Lyon, CNRS, LaMCoS, UMR5259, 69621 Villeurbanne, France

<sup>2</sup> Univ Lyon, INSA Lyon, Université Claude Bernard Lyon 1, Ecole Centrale de Lyon, CNRS, Ampère, UMR5005, 69621 Villeurbanne, France

<sup>3</sup> Univ Lyon, INSA Lyon, LGEF EA682, 69261 Villeurbanne, France

Received: 22 February 2022 / Accepted: 24 June 2022

**Abstract.** The aim of this publication is to conclude on the interest of vibratory energy harvesting on classic quadcopter drone for autonomous applications (battery charging in real time, autonomous sensors), monitoring or even vibration control applications. A complete dynamic analysis allows to quantify the amount of electrical power that is possible to produce during the hovering flight of a quadcopter drone. These results have been obtained by substitution of the inert parts of the drone by piezoelectric components. For that purpose, different types of piezoelectric structures have been tested, including some commercial transducers (DuraAct from Piezoelectric Instrument and Murata buzzers) and some home-made such as a piezoelectric paint. Our original piezoelectric smart arms have been able to scavenge up to 5.35 mW during a stationary flight which remains quite enough to supply low-consumption sensors for monitoring applications.

**Keywords:** Vibration energy harvesting / structural health monitoring / piezoelectricity / plastronic / smart structure / quadcopter drone

## 1 Introduction

Drones and small aircrafts, a class of Unmanned Aerial Vehicle (UAV), sharply widespread from military applications expanding to scientific, agricultural, surveillance or recreative applications. Their main drawbacks remain the relative low in-flight autonomy (from few seconds to hours) and the reduced lifetime requiring new smart technologies to improve these two points. Energy harvesting could be the solution to increase the energetic autonomy by recharging for example the batteries of UAVs. In the state of the art, a dozen of publications can be found on energy harvesting devices embedded on a drone or a small aircraft. In 2002, Fleming et al. [1] presented the results obtained by several thermoelectric (Seebeck) modules on two model aircraft motors. Four VHHFM-2 thermoelectric modules and four heat exchangers placed on a OS MAX 0.61 motor in operation conducted to produce 0.8-1W of electrical power (i.e. 200–250 mW cm<sup>-2</sup>). From 2008 to 2009, Anton et al. published several results obtained with different piezoelectric structures as a clamped-free beam placed inside an small airplane wing [2,3], piezoelectric patches glues on the wings [2–4], as

well as thin-film photovoltaic panels also located on the wings [2,3]. When the aircraft is flying, 11.3 μW (0.69 μW cm<sup>-2</sup>) has been produced by MFC patches (Macro-Fiber Composite), 10.1 μW (0.46 μW cm<sup>-2</sup>) with PFC patches (Piezoelectric Fiber Composite), 24 μW (1.10 μW cm<sup>-2</sup>) with PFC beams and 400mW (823 μW cm<sup>-2</sup>) with thin-film photovoltaic panels. In 2015 and 2016, the publication of Sowah [5] and the patent of Rollefstad [6] mentioned the use of the drone engines as alternators in order to take advantage of the motors rotational mechanical energy. However, the two authors remained relatively unclear on the moments where the electrical energy was actually extracted (landing, change of direction, rotation, etc.) as well as the electrical power levels produced. Some energy harvesters embedded on UAV were also mentioned in [4,7,8] such as piezoelectric devices for the wing vibrations, in [9] as piezoelectric harvesters for the landing, or in [5,6,10] such as rotational electromagnetic systems; but without experimental results. It should also be noted the solutions described in [11–15] for the UAV battery recharge in flight. All these solutions (thermoelectric, solar, piezoelectric, magnetic) underline the potential of energy harvesting on UAVs for recharging batteries or supplying low-consumption systems such as sensors or actuators for health monitoring.

\* e-mail: [simon.chesne@insa-lyon.fr](mailto:simon.chesne@insa-lyon.fr)

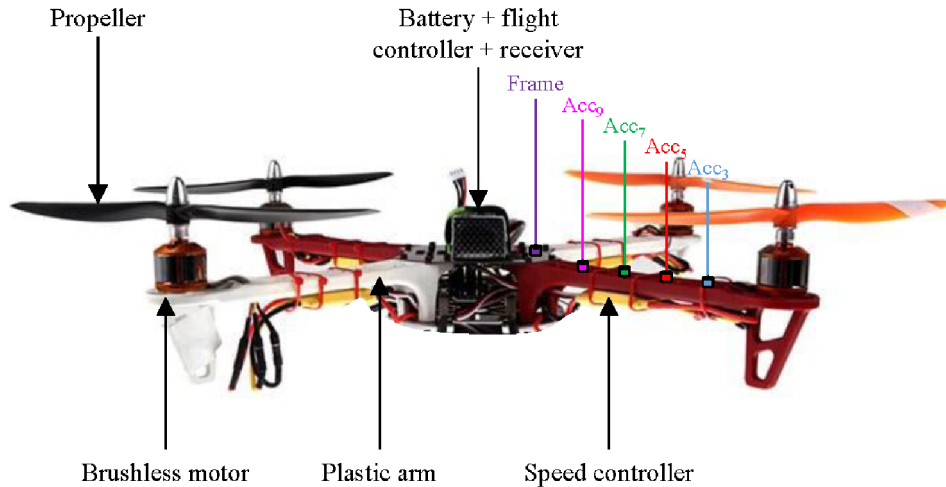


Fig. 1. Picture of a DJI F450 drone and its component parts.

Excluding solar intermittent energy, the vibrations remain the main source of energy on UAVs. A complete dynamic analysis on a classic drone, namely a quadcopter drone, is required to firstly quantify the amount of energy that is possible to produce during a flight and to clearly define the potential applications on UAVs: recharging batteries to increase the in-flight time, supplying sensors for embedded monitoring leading to higher lifetime of the structure or vibration control applications to increase the stability of the drone or the stability of embedded equipment such as cameras. In this task, let's underline the research work done in [16–20] on the dynamics of different drones.

Finally, one can also note that a low-weight and space-saving solution is required for UAVs leading to integrated solution such as smart composites or plastronic system. Piezoelectric transducers are thus well-suited for integration into complex structures [21] and piezoelectric material can be directly deposited on or into specific parts of the system, thus adding an active function to classic inert/passive structural parts of the system. Thus, one of the originalities of our study is the modification and analysis the drone by replacing an inert structural part of this quadcopter drone by an active structural part including piezoelectric transducers used for example for energy harvesting application. It illustrates the possibility of functionalizing (monitoring, harvesting, controlling, etc.) such a structure by performing an energy and dynamic balance.

This paper includes firstly an experimental modal analysis performed on a quadcopter DJI F450 drone, the quantification of the effects of the main vibrations source (strain of structural parts) and the design of the active structural part which allow to incorporate piezoelectric structures while keeping a similar dynamic behavior. A vibratory analysis in real conditions of this original active structure will be presented, and the experimental results on energy harvesting level obtained with different types of piezoelectric structures will be discussed.

## 2 Initial structure and evolutions

A DJI F450 quadcopter drone is investigated (Fig. 1). This drone is very simple to assemble/disassemble with an

affordable price and is widely distributed on the market. It will therefore be very easy to replace a standard part of the drone by a functionalized part including piezoelectric transducers. The DJI F450 drone is composed of a central frame on which is mounted four plastic arms of 45.9 g each. On each arm is placed a speed controller of 28.9 g, a brushless motor of 52.7 g and a 12.6 g propeller. On the central frame, a FS-IA6B receiver of 15.8 g can be found, a 28.0 g APM 2.8 flight controller and a HRB lithium battery (412 g for the 6000 mAh = 21.6 kJ battery or 169 g for the 2600 mAh = 9.36 kJ battery) complete this drone.

As the aim of this research work is to quantify the level of harvested vibration energy during the different phases of a flight, the first step was to identify the most loaded areas of the chosen DJI 450 quadcopter drone. Whatever the operation of the drone (rising phase, hovering flight, spin turning in place, etc.), the four electrical motors are the main source of the vibratory excitation measured into the different parts of the structure, vibrations which could be mode shape of the structure or harmonic of the excitation. Thereafter, as the acceleration levels tend to logically increase when approaching the motors, we focused our study on functionalizing the arm of the drone by adding piezoelectric structures on these arms.

The initial arms of the DJI F450 drone weight 45.9 g and are made of polymer with a Young modulus experimentally measured at 2.5 GPa (value issued from the first resonance frequency in a clamped-free configuration and Finite Element analysis). In order to include piezoelectric elements on the arms of the drone and as we want to take advantage of the out-of-plane bending of the arms, the geometry of the arms have been adapted (from Fig. 2a to Fig. 2b and its overview in Fig. 3). This simple shape ensures a significant area to place several piezoelectric structures, area three time larger than the one in the initial arm (45 cm<sup>2</sup> compared to 15 cm<sup>2</sup> on each side). The different attachment points for the central frame and the motors remain identical, the clamping part is slightly widened to avoid any mechanical failures. It remains to be seen which thickness is necessary to keep a quasi-equivalent stiffness/dynamic of the revised arm. Three

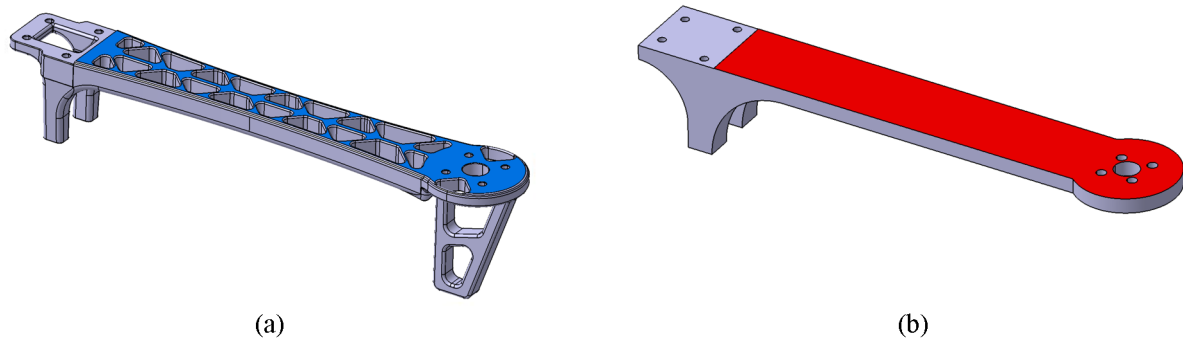


**Fig. 2.** (a) Initial arm: 218 mm in total length, variable width 24–31 mm (blue area: approximately  $15 \text{ cm}^2$  on each side). (b) Revised arm: 218 mm in total length, 31 mm width (red area:  $45 \text{ cm}^2$  on each side).

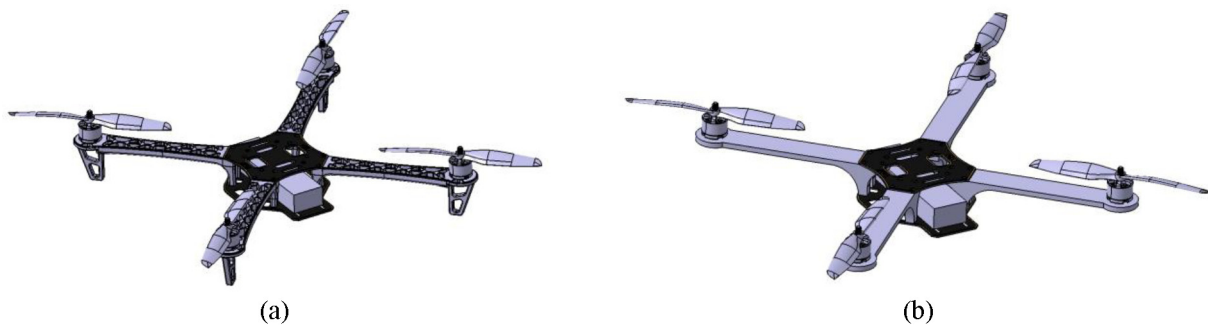


**Fig. 3.** Isometric view of the (a) initial drone and the (b) revised drone.

different thickness have been tested (4, 5 and 6 mm). The modified arms have been made of acrylic resin by stereolithography in Ampère laboratory, in order to simplify the electrodes deposition. The density of this material is  $1230 \text{ kg m}^{-3}$  with a Young modulus of 2.5 GPa, based on experimental measurements carry out by the Ampère laboratory. It may be noted that this manufacturing process is a first step (the process is now mastered), future works will be focused on the use of plastronic technologies and on the integration of composite materials. Different arms were fabricated to best fit the actual dynamic behavior of the structure, the resulting vibration, being a balance between the bending stiffness and the added mass.

- The mass of the 4 mm-thick arm is equal to 48 g (compare to the 45.9 g of the initial arm) for a static stiffness of  $0.328 \text{ N mm}^{-1}$  (calculated with Ansys<sup>®</sup>).
- The mass of the 5 mm-thick arm is equal to 54 g for a static stiffness of  $0.613 \text{ N mm}^{-1}$ .
- The mass of the 6 mm-thick arm is equal to 61 g for a static stiffness of  $1.022 \text{ N mm}^{-1}$ .

### 3 Dynamic analysis of the drone

#### 3.1 Single arm modes

The energy available to be harvested is directly related to the vibrational behavior of the structure, in terms of amplitude and spatial distribution. To quantify these energy levels, it is important that the new instrumented arm has a very similar dynamic behavior. In order to better

understand the dynamic of the arms, an experimental modal analysis is firstly done on an arm in a clamped-free configuration, as illustrated in Figure 4a. The vibratory excitation is performed by a B&K LDS V408 shaker fixed to the free end of the arm, and the injected force is measured thanks to a force sensor B&K 8200 (Fig. 4a). Four B&K 4517 drop charge accelerometers have been chosen for their lightweight (0.7 g each), in order to restrict their impact on the dynamic of the arm.

The four accelerometers were firstly placed on the upper part of the initial arm (positions named Acc<sub>3</sub>, Acc<sub>5</sub>, Acc<sub>7</sub> and Acc<sub>9</sub> in Fig. 4a) and secondly on the lateral part (positions called Acc<sub>13</sub>, Acc<sub>15</sub>, Acc<sub>17</sub> and Acc<sub>19</sub> in Fig. 4a) to identify the various modes between 0 and 1000 Hz.

Three “out-of-plane” bending modes (Fig. 4b), two “in-the-plane” bending modes and one torsional mode have been found in the chosen frequency range. Regarding the bending modes, an experimental analysis with a Laser Doppler Vibrometer (Polytech PSV-400) allow us to properly identify the shape of the mode, as illustrated with the small enclosed images in Figure 4b. This mode shape identification is in complete agreement with the measured level of acceleration done by the four accelerometers placed on the top of the arm. The three bending frequencies are respectively: 50 Hz, 515 Hz and 930 Hz. As expected, one can also note that as classically observed for clamped-free configuration, the highest level of strain is observed near the clamped edge. This observation will be verified for the entire drone assembly in the next parts. Figure 5a introduces the four Frequency Response

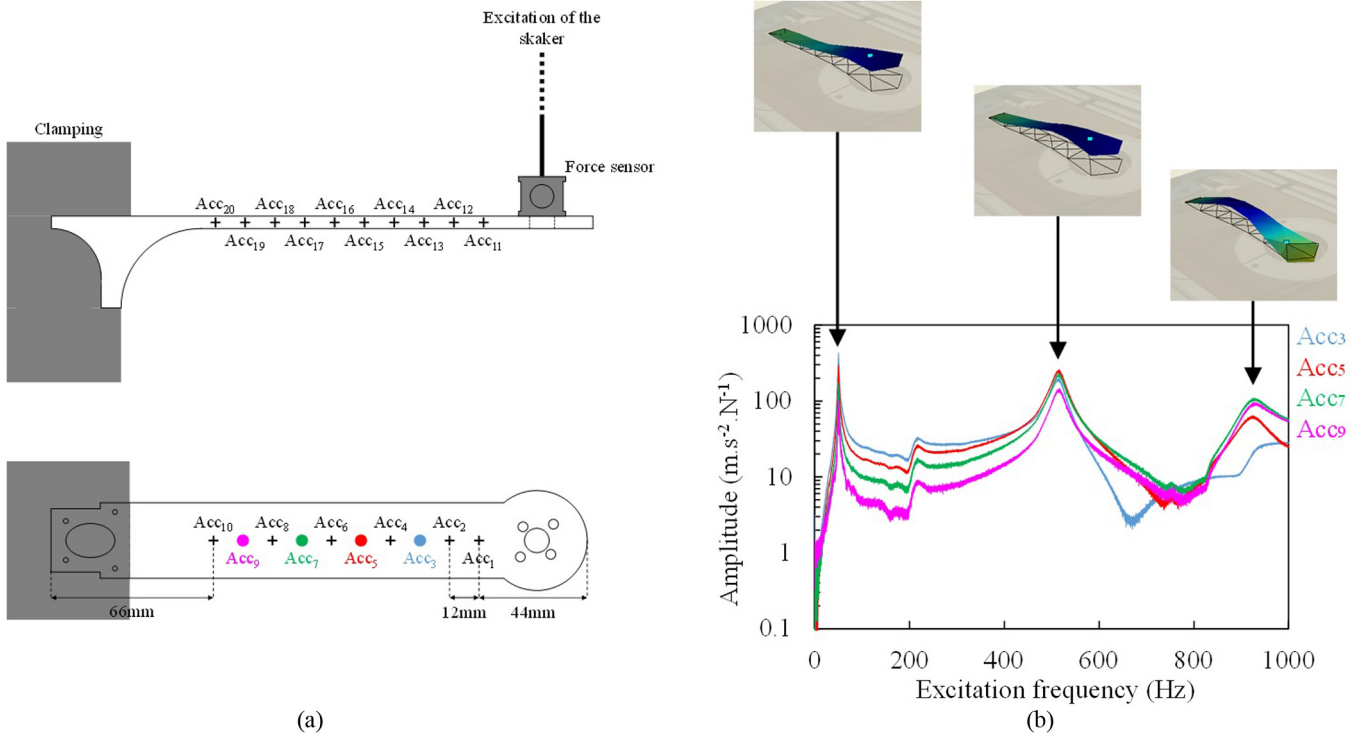


**Fig. 4.** (a) Set up use to characterize the arms and localization of the different accelerometers on the revised arm. (b) Identification of the first three “out-of-plane” bending modes of the initial arm. Frequency Response Function (FRF) measured by injecting a white noise at the free end of the initial arm.

Functions (FRFs) related to the initial arm and the three revised arms (4 mm, 5 mm and 6 mm). It may be observed that the 6 mm-thick arm develops the nearest behavior compared to the initial arm, with especially a very good fit on the first mode frequency (Fig. 5b). In the rest of this paper, this particular 6mm arm will be used as revised arm.

### 3.2 Global modes of the drone

Experimental modal analysis of the initial drone and of the drone with 6 mm arms have been achieved following the method described in the previous sub-section for the dynamic analysis of a single arm. A B&K LDS V408 shaker is placed on the workbench and provide a white noise excitation at the center of the frame of the drone and four accelerometers B&K 4517 are located on one arm ( $Acc_3$ ,  $Acc_5$ ,  $Acc_7$ ,  $Acc_9$ ). An additional accelerometer (B&K 4381) is fixed on the frame near the center of the drone. All parts of the drone (motors, battery, controllers, etc.) are assembled and the electrical motors are all off. A Laser Doppler Vibrometer (Polytech PSV-400) was also used to define precisely the mode shape of the structure. A precise mapping of the drone with reflective point is thus realized. Contrary to previous experiments, the drone is in “free-free” conditions, namely it has been hung thanks to four elastics fixed to the base of the four arms. Figure 6 describes the experimental set-up for the drone with the 6 mm revised arms.

Figure 7a shows the FRFs related to five accelerometers. This “free-free” configuration allows to highlight two out-of-plane bending modes: the first one at 35 Hz and the second one

at 60 Hz. At higher frequency, other modes might be present but it can be seen that they are largely damped. Thanks to the various accelerometers and the velocimeter measurements, it can be observed that the four arms are bending in phase for these two modes, as plotted in the embedded images in Figure 7. The modal shape of the first mode (35 Hz) presents a node located between  $Acc_5$  and  $Acc_7$  contrary to the modal shape of the second mode (60 Hz) which has no node. As can be expected, the revised drone with the 6 mm arms, exhibits a very similar behavior with a first resonance frequency at 28 Hz and the second one at 49 Hz. The modal shapes of the revised drone are similar to the initial one as it can be seen in Figure 7b. It is also interesting to note that for the same vibratory excitation, the level of vibrations is higher on the revised drone than on the initial one, leading to higher level of strain on the revised arms which is quite interesting for our application with piezoelectric elements (Fig. 7b). As expected, the highest levels of curvature are observed near the central part of the drone. Moreover, these figures show that with the new instrumented arms, the drone presents a very similar vibratory behavior to the initial one.

## 4 Operational condition analysis: Drone in hovering flight

In order to carefully test the drone in hovering flight, a dedicated test bench has been designed and manufactured (Fig. 8a). This cage is composed of an aluminum frame and aluminum panel. During the tests, the cage is completely



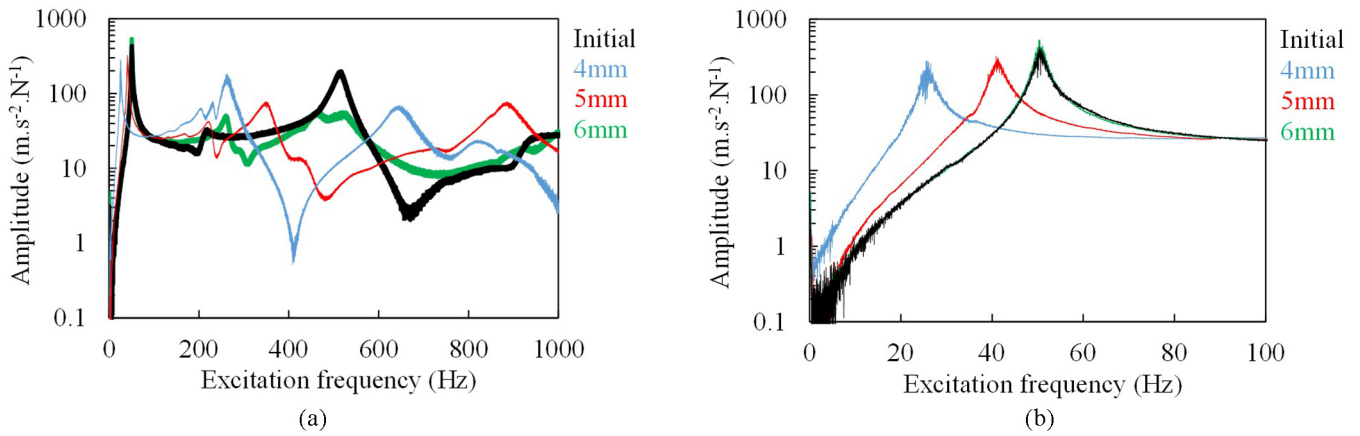


**Fig. 5.** Comparison of the FRF between the initial arm and the revised arms using the accelerometer Acc3: (a) FRF between 0 and 1000 Hz, (b) focus on the first mode.

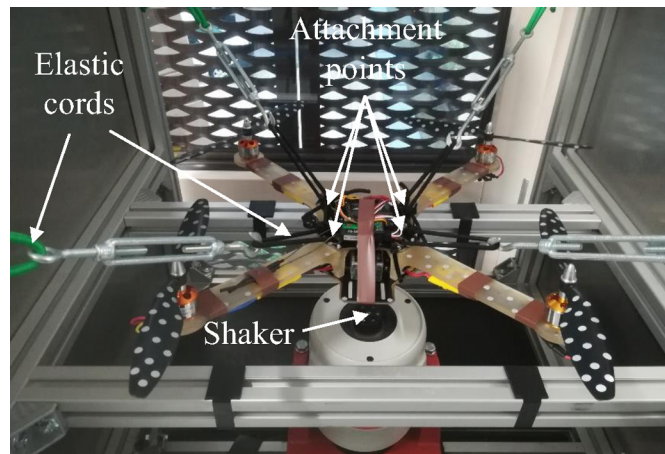


**Fig. 6.** Installation of the revised drone in “free-free” conditions, the motors were off.

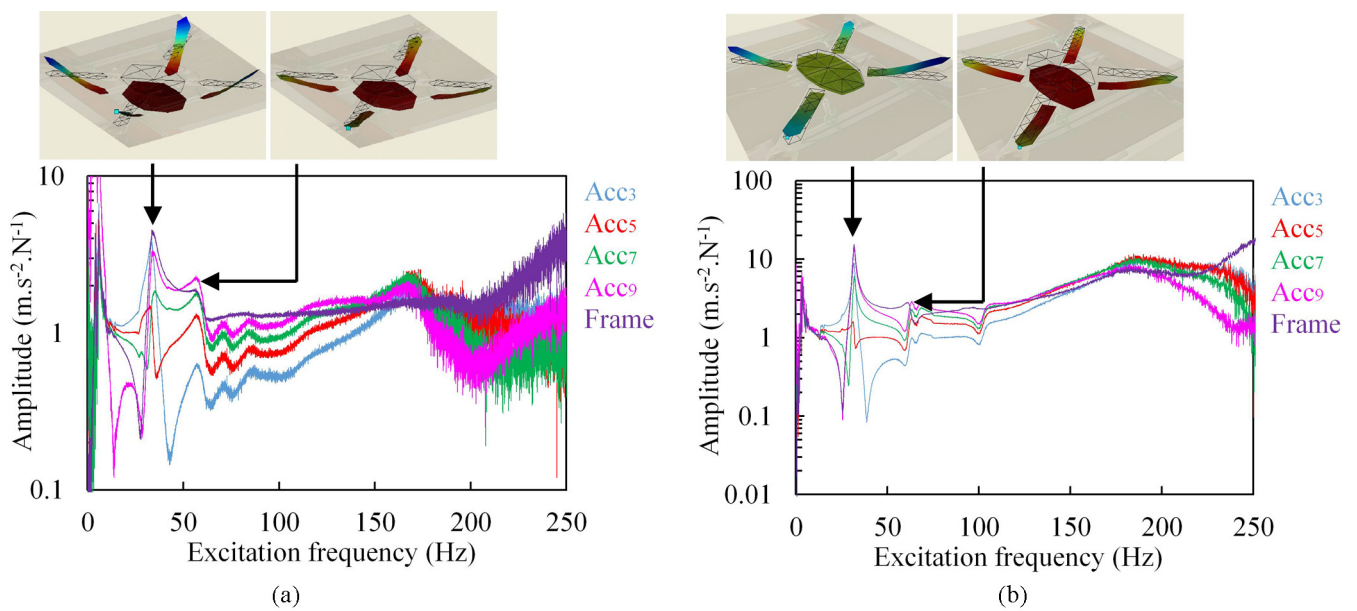


**Fig. 7.** FRF computed by injecting a white noise at the center of the (a) initial drone and the (b) revised drone, both without propeller.

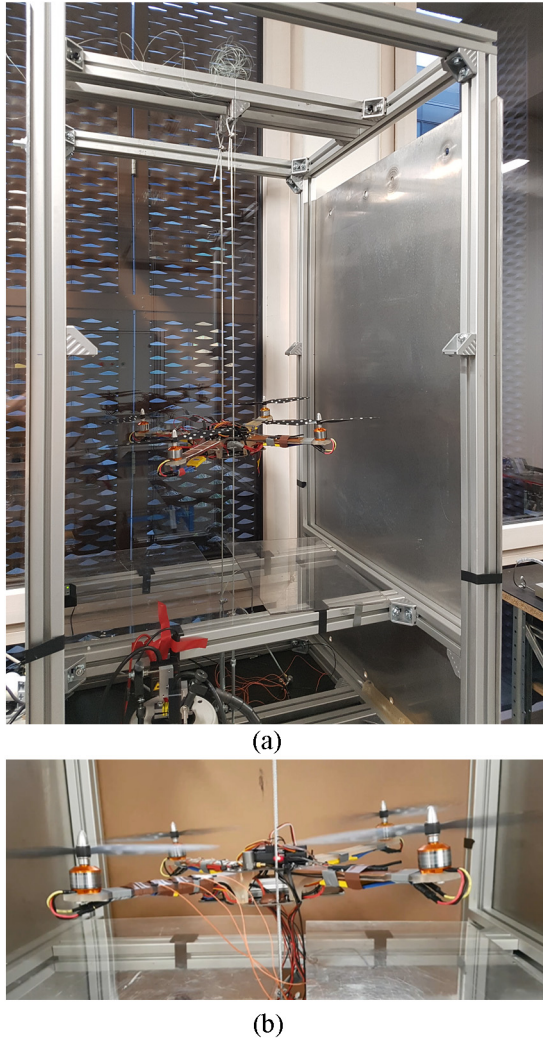


**Fig. 8.** (a) Cage used to test the different drones under real conditions and (b) revised drone in hovering flight.

closed. Only a small area is let opened to check the correct running of experiments. This cage is big enough (80 cm × 80 cm × 150 cm) to let the drone fly inside under operational condition. The drone can be left free or driven by two cables as presented in Figure 8a and 8b. The drone can then slide safely before stabilizing in hovering flight. As realized in the previous experiments, four low-weight accelerometers are located on one arm on of the drone (Acc3, Acc5, Acc7 and Acc9 as described in Fig. 4a) and another one is place in the frame in the center of the drone. All parts of the drone (motors, battery, controllers, etc.) are assembled and the electrical motors are all on to simulate a hovering flight. Several masses can also be added into the drone in order to simulate additional equipment such as a camera, a GPS, an extra battery, etc. Finally, the rotational speed of the motors can be measured thanks to a laser sensor focused on a blade.

Figure 9a and 9b provides the Power Spectral Densities (PSDs) measured at different locations of one arm and on the frame (Fig. 1) for two different embedded masses: battery and battery plus additional mass. On these two

figures, it can be highlighted that the excitation is wide band excitation with a first fundamental frequency related to the rotational speed of the motor and its harmonics. The increase of the embedded mass (additional mass of 400 g) on the drone tends to increase the rotational speed of the motors (from 72 Hz to 78 Hz) and as a consequence increase the whole excitation frequencies. Nevertheless, even if the mass of the drone is set at its minimum, the fundamental frequency directly related to the rotational speed of the motors remains significantly higher than the first natural frequency of the drone: 72 Hz in Figure 9a vs 28–35 Hz in Figures 5b and 7b. In this configuration, the harmonic perturbations generated by the motors will not coincide with the drone dynamic. Avoiding this frequency coincidence is a common constraint in mechanical engineering. But many harvesting devices require mass addition through an auxiliary oscillating system. Obviously, such additions are not possible in the realistic case where the host structure is very light. Therefore, the harvesting device cannot benefit from the vibration amplification due to the resonant frequency (except during short moments of engine acceleration or deceleration). This observation being made, the rest of the paper will focus on the non-optimal case of hovering where the perturbations are stable.

## 5 Functionalization of the drone: piezoelectric transducers on the arms

Thanks to our previous complete dynamic analysis, we demonstrate that during a hovering flight, no specific structural mode of the drone will be stimulated. The vibration excitation of the drone due to the electrical motors is thus a wide range excitation meaning that the level of strain into the arms will be relatively low and that various structural out-of-plane bending modes could be solicited. One can remember that the piezoelectric transducers need high level of strain to generate high level of charges, leading to the segmentation of the arm in different areas in which the piezoelectric transducers will be deposited or glued.

Through the example of two piezoelectric structures taped on each side of a beam loaded in out-of-plane bending (Fig. 10), if the thickness of the piezoelectric and electrode layer is negligible compared to the thickness of the substrate, then the following simplified equation can be written:

$$D_3 = d_{31}T_{11} + \epsilon_0\epsilon_{33}E_3 \quad (1)$$

with  $D_3$  the electric displacement field in the  $e_3$  direction,  $T_{11}$  the stress applied to the face 1 in the  $e_1$  direction,  $E_3$  the electric field in the  $e_3$  direction,  $d_{31}$  one of the piezoelectric coefficients,  $\epsilon_0$  the permittivity constant of vacuum,  $\epsilon_{33}$  the relative permittivity related to the  $e_3$  direction. This shows the main parameters that affect performance.

As the levels of strain and stress are relatively low in the arm, the entire surface of the arm will be covered with piezoelectric transducers in order to increase the output level of harvested energy. One can easily understand that the piezoelectric transducer located near the central part of

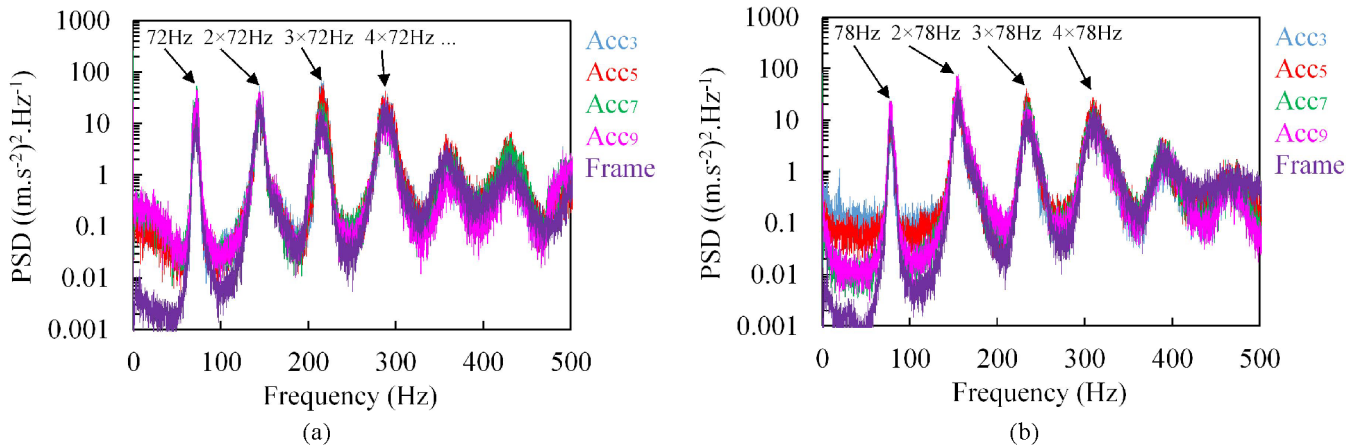


**Fig. 9.** PSD measured during a hovering flight: (a) 2600 mAh battery (169 g), (b) 2600 mAh battery (169 g) + 400 g.

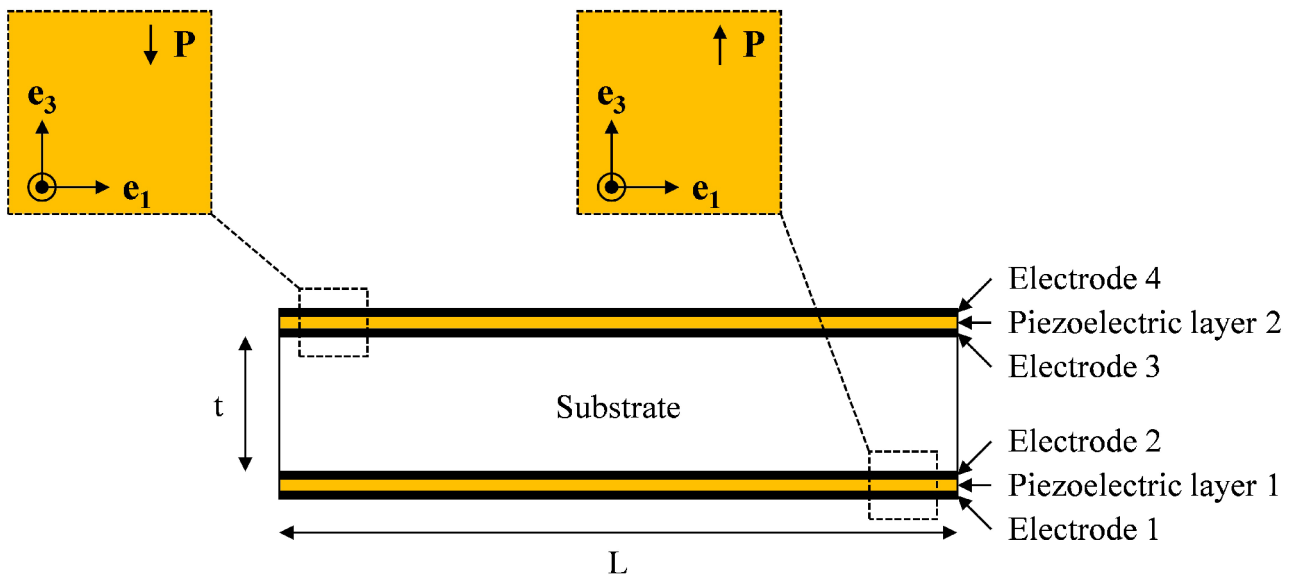


**Fig. 10.** Section view of a functionalized beam structure.

the drone (called frame) will be more deformed as this part of the arm undergoes larger strain, even in a “free-free” configuration as previously underlined in our experiments. The displacement fields represented in Figure 7 also show the high curvature level near the central part. Three different piezoelectric transducers are used in our experiments to functionalize the arms: two commercial ones (PI and Murata) and one home-made (piezoelectric paint). The home-made piezoelectric transducers are deposited using classic technic. Firstly, a  $5\ \mu\text{m}$ -thick copper layer has been deposited by electroless metallization in the Ampère laboratory on the whole upper and lower face of each arm (Fig. 11a). The spray deposition of the piezoelectric layer ( $120\ \mu\text{m}$  of Polyurethane /BaTiO<sub>3</sub>) is then realized by the LGEF laboratory, as illustrated in Figure 11b in order to

cover entirely the first copper layer [22]. Only two output pins enable to connect this first layer of electrodes to the ground. Finally, eight 35 mm-width copper electrodes ( $5\ \mu\text{m}$  in thickness) have been deposited by electroless metallization directly on the piezoelectric layer in order to exploit the entire surface of the arm (Fig. 11c). The piezoelectric structures are finally polarized at 480 V ( $4\ \text{V}\ \mu\text{m}^{-1}$ ) in a heat chamber maintained at  $90\ ^\circ\text{C}$ . Thereafter, the facing electrodes could be associated with the same resistive load since they will be subject to the opposite deformations.

Finally, two other arms have also been equipped with commercial piezoelectric structures. Overall, seven Murata buzzers were glued on the first arm (3.5 g each: Fig. 12a) as well as three other PI DuraAct 876.A15 patches (7.2 g each: Fig. 12b).



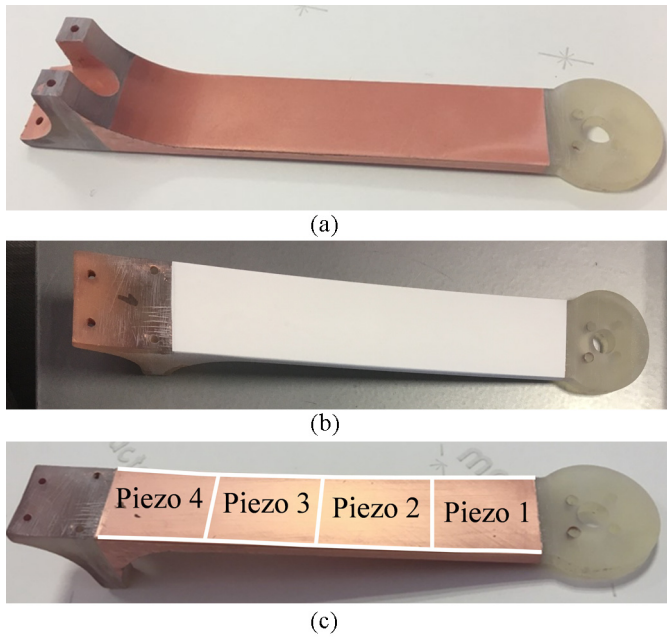


**Fig. 11.** Manufacturing steps of the “integrated piezoelectric arm”: (a) after deposition of the first copper layer (Ampère), (b) after deposition of the piezoelectric layer (LGEF), (c) after deposition of the second copper layer (Ampère).

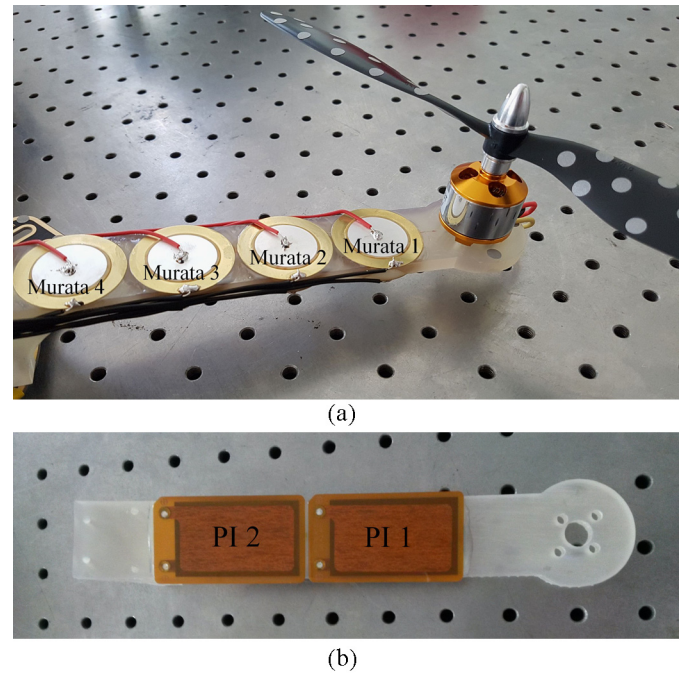


**Fig. 12.** Integration of commercial piezoelectric structures: (a) Murata buzzers, upper side of the arm, (b) PI DuraAct 876.A15 patches, upper part of the arm.

## 6 Results and discussion on the harvested energy

### 6.1 Characterization of the functionalized arms

As a first step, a characterization of the arms alone is done. The different functionalized arms with piezoelectric structures were tested in a free-clamped configuration under a mono-harmonic excitation. Even if this situation differs slightly from the real case, it represents a test case for comparison. A sinusoidal force (amplitude 0.1 N), closed to the first mode of resonance of the structure, was injected at the free end of the arm thanks to an electromagnetic shaker (see Sect. 2; Fig. 4) and the electrical power produced was measured for different resistive loads by computing the square of the piezoelectric output voltage divided by the resistance value. Figure 13 highlights the average electrical output power harvested with a single Murata ceramic (Fig. 12: Murata 4) and with the home-made piezoelectric layer (Fig. 11: Piezo 4). These two transducers, located closest to the clamped end of the arm (Figs. 11 and 12), sustain the highest level of strain in a clamped-free configuration, leading to higher level of harvested energy.

The commercial Murata piezoelectric transducer harvests almost  $3.5 \mu\text{W}$  on an optimal resistive load of  $90 \text{ k}\Omega$ , while the home-made piezoelectric transducer harvests  $1.5 \mu\text{W}$  on an optimal resistive load of  $800 \text{ k}\Omega$ . One can note that the output electrical power harvested by the two piezoelectric transducers are in the same range (few  $\mu\text{W}$ ) while Murata are heavy and rigid and our home-made

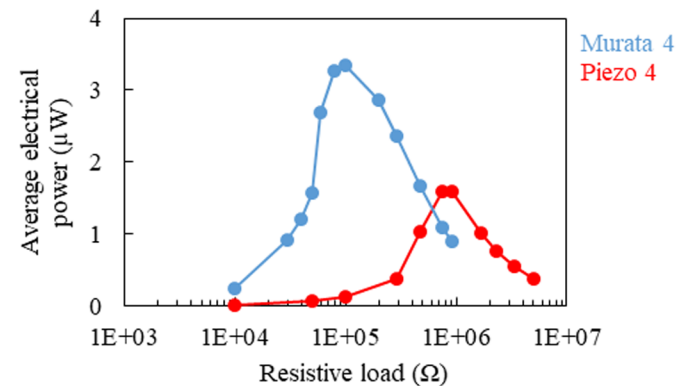


**Fig. 13.** Harvested electrical energy with a commercial piezoelectric transducer (in blue) and with our home-made one (in red).

transducer are very light and compliant (density of the piezoelectric paint of about  $2.2 \text{ g cm}^{-3}$ ). Note that for this type of application (very light flying structure), the structural modification of the host structure due to the addition of transducers should be as small as possible. It is therefore preferable to use light and flexible transducers. The maximal harvested power density per transducer are thus respectively  $1 \mu\text{W g}^{-1}$  and  $3.9 \mu\text{W g}^{-1}$  underlying the promising performance of our home-made piezoelectric transducers. The dynamic of the functionalized arm with the piezoelectric paint, is exactly the same as the initial arm with a first bending resonance at 50 Hz as the thin layers of active material and electrodes add a very small mass and

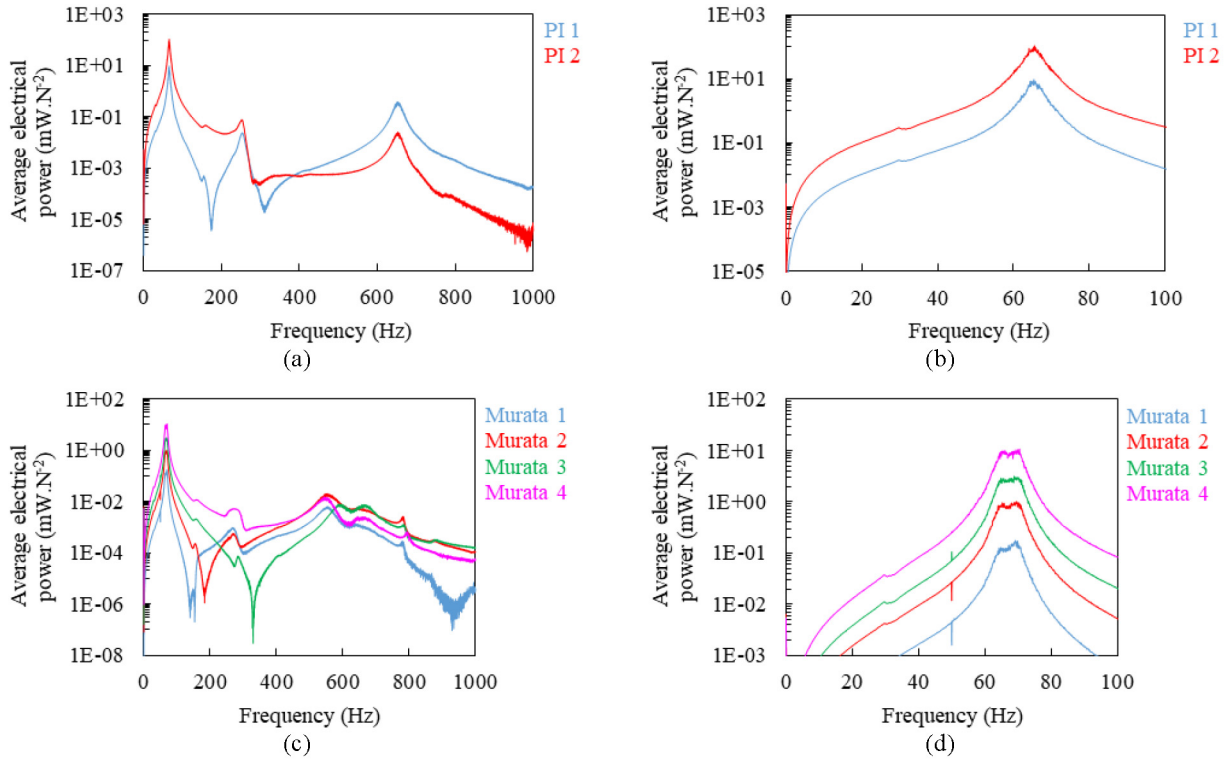


**Fig. 14.** (a) and (c) Transfer function of the different piezoelectric structures by injecting a white noise at the free end of the arm (the other end is clamped). Integrated structures:  $R = 200 \text{ k}\Omega$ , Murata buzzers:  $R = 100 \text{ k}\Omega$ , PI DuraAct patches:  $R = 70 \text{ k}\Omega$ . (b) and (d) Zoom on the first mode.

stiffness to the arm. Unfortunately, the numerous tests put a lot of strain on these prototypes, and the piezoelectric paint showed damages mainly due to delamination. It was not possible to perform more extensive flight tests for these transducers (next section).

The addition of Murata buzzers ( $7 \times 3.5 \text{ g}$  of added mass) induced a significant increase of the arm stiffness, which induced a frequency offset respectively of  $+17 \text{ Hz}$  (for the first considered mode), and the PI piezoelectric patches ( $3 \times 7.2 \text{ g}$  of added mass) induces a frequency offset of  $+15 \text{ Hz}$ , as it is clearly stated in Figure 14. Figure 14 highlights the transfer functions (electric power/square force) of the different structures with commercial piezoelectric transducers and demonstrates that the areas closest to the clamping are the most interesting. As explained in Section 2, a white noise was injected at the free end of each arm and the electrical power produced was measured for different resistive load by computing the square of the piezoelectric output voltage divided by the resistance value. We verified that the electric voltage produced by each piezoelectric patch was proportional to the injected force, which allows to nondimensionalize the electrical power by the force injected square.

Regarding the arm equipped with PI DuraAct 876.A15 patches, an electrical power of  $9.17 \text{ mW N}^{-2}$  on the PI 1 patch and  $117 \text{ mW N}^{-2}$  on the PI 2 patch (nearest to the clamping) were respectively produced. For the Murata buzzers, the following levels of electrical power

were measured:  $190 \mu\text{W N}^{-2}$  on the Murata 1 buzzer,  $1.07 \text{ mW N}^{-2}$  on the Murata 2 buzzer,  $3.16 \text{ mW N}^{-2}$  on the Murata 3 buzzer and  $10.8 \text{ mW N}^{-2}$  on the Murata 4 buzzer. The PI DuraAct are made of modified Lead Zirconate Titanate (PZT), called ceramic PIC255, with a piezoelectric coefficient  $d_{31}$  equal to  $-180 \text{ pC N}^{-1}$  which is higher than the one of our home-made piezoelectric transducer ( $d_{33} \approx 3 \text{ pC N}^{-1}$ ).

## 6.2 Achievement in hovering flight

Figure 15 reports the levels of harvested electrical power with commercial piezoelectric transducers, recorded during the hovering flight of the drone with a 2600 mAh battery, on different resistive loads. It can be seen that the piezoelectric elements which are closest to the central part of the drone, namely PI 2 and Murata 4 (see Figs. 11 and 12 for localization) produce the highest levels of electrical power. An average electrical power of  $4.4 \mu\text{W cm}^{-2}$  was achieved for the Murata buzzers, and  $14.9 \mu\text{W cm}^{-2}$  for PI DuraAct 876.A15 patches. As previously measured in the “clamped-free” configuration, the PI transducers harvest the highest level of energy even under a wide vibratory excitation.

As the total area of the four arms (upper and lower parts) is equal to  $359.6 \text{ cm}^2$ , we can thus extrapolate the following levels of harvested electrical power:  
 –  $1.58 \text{ mW}$  by covering the four arms with Murata buzzers.

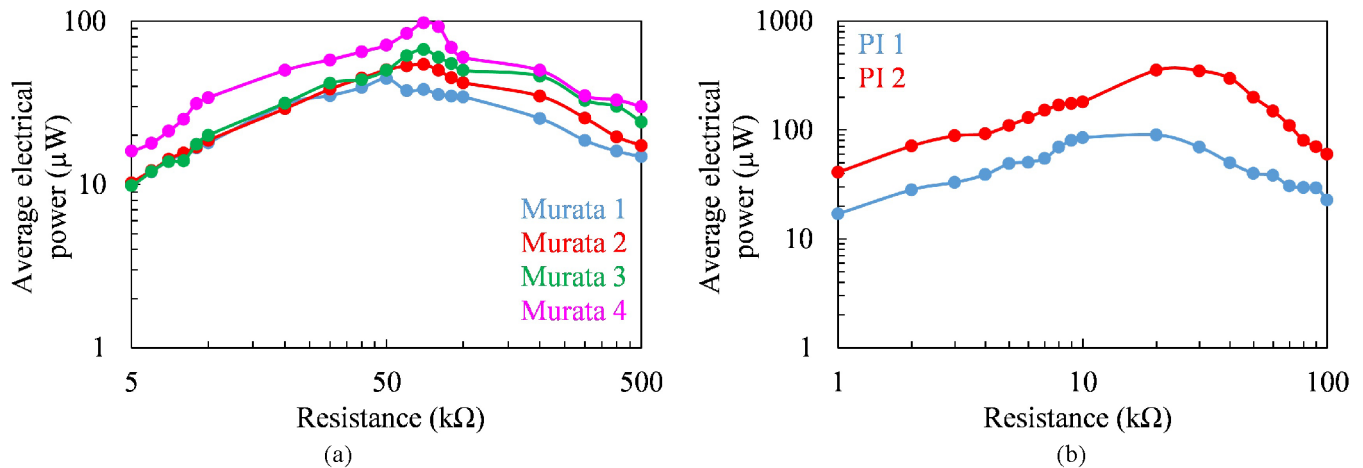


**Fig. 15.** Average electrical power produced by different piezoelectric structures during a hovering flight, with a 2600 mAh (169 g) battery: (a) Murata buzzers, (b) PI DuraAct 876.A15 patches.

- 5.35 mW by covering the four arms with PI DuraAct 876.A15 patches.

Practically, a 2600 mAh battery allows the drone to fly during approximately 10 min. In that respect, it can be concluded that the drone requires a continuous power of 15.6 W to maintain a hovering flight. Then, the following gains in flight time due to the harvested electrical power, can be extrapolate:

- 0.061 s for a 10 min hovering flight with Murata buzzer.
- 0.21 s for a 10 min hovering flight PI DuraAct 876.A15 patches.

Clearly, these added times of flight are very low ( $<s$ ) and unusable in practical applications. Nevertheless, the level of harvested electrical power with the commercial piezoelectric transducers remains quite interesting ( $>mW$ ) and high enough to supply various low-consumption sensors such as an accelerometer or a temperature sensor used for monitoring applications. Indeed, an autonomous sensor node generally needs at least  $100\ \mu W$ – $1\ mW$  to measure (not in continuous), process and send an information [23]. The home-made piezoelectric transducers develop level of harvested energy in the same range as the Murata buzzer (Fig. 13) but are up to now, too fragile for hovering flight experiments as delamination issues occurred during our tests. Nevertheless, this plastronic technology offer promising performance in term of potential harvested energy and integration. Indeed, active piezoelectric layers could be directly developed and deposited during the fabrication process of the drone. This integration property is a tremendous advantage to design embedded sensors such as strain sensor or force sensor that could be used in monitoring application especially in structure health monitoring applications, or to design transducers for harvesting applications. Many parameters must be optimized to improve performance such as transducer thickness (depending on the type). Finally, the present electrical powers were measured on a simple passive impedance matching, but using an active power management circuit would allow to obtain much better results [24].

## 7 Conclusions

This paper exhibited for the first time in the state of the art, a complete dynamic analysis of a quadcopter drone and the analysis of the electrical power levels produced by the vibrations of this drone during a hovering flight. Classic passive structural parts of the drone have been functionalized to integrate a harvesting function, through the use of piezoelectric elements. Two commercial piezoelectric transducers and one home-made have been employed to functionalize the arm of the drone, while keeping a similar dynamic behavior and without increasing the levels of mechanical vibrations. From our original experiments and extrapolations, it can be expected that the levels of power reached with piezoelectric transducers ( $>mW$ ) are sufficient to supply a sensor for SHM applications for example, but certainly not for the purposes of increasing the flight time of the drone. The home-made piezoelectric transducers underline strong promising performances as the harvested power remains in the same range as the commercial piezoelectric transducers, and need further developments to improve their adhesion to the host structure and thus their lifetime.

*Acknowledgements.* The authors would like to thank the Carnot Institute “Ingénierie à Lyon” for its support and funding through the project Metafab-3D.

## References

- [1] J. Fleming, N. Wing, Thermoelectric-based power system for UAV/MAV applications, Technical conference and workshop on unmanned aerospace vehicles (2012)
- [2] S.R. Anton, A. Erturk, D.J. Inman, Energy harvesting from small unmanned air vehicles, Int. Symp. Appl. Ferroelectr. (2008)
- [3] S.R. Anton, D.J. Inman, Vibration energy harvesting for unmanned aerial vehicles, Active and passive smart structures and integrated systems (2008)

- [4] S.R. Anton, D.J. Inman, Novel piezoelectric energy harvesting devices for unmanned aerial vehicles, Open Source (2009)
- [5] R. Sowah, M.A. Acquah, A.R. Ofoli, G.A. Mills, K.M. Koumadi, Rotational energy harvesting to prolong flight duration of quadcopters, *Trans. Ind. Appl.* (2015)
- [6] S.B. Rollefstad, Unmanned aircraft system (UAS) with active energy harvesting and power management, US patent (2016)
- [7] P.B. MacCready, Regenerative battery-augmented soaring, Self-launching Sailplane Symposium (1998)
- [8] K.C. Magoteaux, B. Sanders, H.A. Sodano, Investigation of an energy harvesting small unmanned air vehicle, *Active and passive smart structures and integrated systems* (2008)
- [9] A. Erturk, J.M. Renno, D.J. Inman, Modeling of piezoelectric energy harvesting from an L-shaped beam-mass structure with an application to UAVs, *J. Intell. Mater. Syst. Struct.* (2009)
- [10] A. Chakrabarty, J.W. Langelaan, Flight path planning for UAV atmospheric energy harvesting using heuristic search, *Guidance, navigation, and control conference* (2010)
- [11] J.M. Arteaga, S. Aldhafer, G. Kkelis, C.H. Kwan, D.C. Yates, P.D. Mitcheson, Dynamic capabilities of multi-MHz inductive power transfer systems demonstrated with batteryless drones, *Trans. Power Electr.* (2014)
- [12] V. Bonnin, E. Benard, J.M. Moschetta, C.A. Toomer, Energy-harvesting mechanisms for UAV flight by dynamic soaring, *Atmos. Flight Mech. Conf.* (2015)
- [13] S. Aldhafer, P.D. Mitcheson, J.M. Arteaga, G. Kkelis, D.C. Yates, Light-weight wireless power transfer for mid-air charging drones, *European Conference on Antennas and Propagation* (2017)
- [14] P.D. Mitcheson, D. Boyle, G. Kkelis, D.C. Yates, J.A. Saenz, S. Aldhafer, E. Yeatman, Energy-autonomous sensing systems using drones, *Sensors* (2017)
- [15] A. Raciti, S.A. Rizzo, G. Susinni, Drone charging stations over the buildings based on a wireless power transfer system, *Industrial and Commercial Power Systems Technical Conference* (2018)
- [16] Y.K. Yap, Structure health monitoring for unmanned aerial systems, *Master of Engineering* (2014)
- [17] A. Coulon, R. Augez, C. Clerc, F. Morra, Approche calcul/mesure pour l'optimisation dynamique d'un drone, 22eme congres francais de mecanique (2015)
- [18] D.K. Schmidt, W. Zhao, R.K. Kapania, Flight dynamics and flutter modeling and analyses of a flexible flying wing drone, *Atmospheric Flight Mechanics Conference* (2016)
- [19] J. Verbeke, S. Debruyne, Vibration analysis of a UAV multirotor frame, *International conference on noise and vibration Engineering* (2016)
- [20] A. Martinetti, M. Margaryan, V.D. Dongen, Simulating mechanical stress on a micro unmanned aerial vehicle (UAV) body frame for selecting maintenance actions, *Proc. Manufactur.* (2018)
- [21] S. Chesné, C. Jean-Mistral, L. Gaudiller, Experimental identification of smart material coupling effects in composite structures, *Smart Mater. Struct.* (2013)
- [22] J.-F. Capsal, C. David, E. Dantras, C. Lacabanne, Piezoelectric sensing coating for real time impact detection and location on aircraft structures, *Smart Mater. Struct.* (2012)
- [23] M. Perez, S. Boisseau, M. Geisler, G. Despesse, J.L. Reboud, A triboelectric wind turbine for small-scale energy harvesting, *J. Phys.: Conf. Ser.* (2016)
- [24] M. Perez, S. Boisseau, M. Geisler, P. Gasnier, J. Willemin, G. Despesse, J.L. Reboud, Aeroelastic flutter energy harvesters self-polarized by triboelectric effects, *Smart Mater. Struct.* (2018)

**Cite this article as:** M. Perez, K. Billon, T. Gerges, J.F. Capsal, M. Cabrera, S. Chesné, C. Jean-Mistral, Vibration energy harvesting on a drone quadcopter based on piezoelectric structures, *Mechanics & Industry* **23**, 20 (2022)